Meteoritics & Planetary Science 39, Nr 7, 1089–1098 (2004)
Abstract available online at http://meteoritics.org

Stratigraphic and sedimentological observations from seismic data across the Chicxulub impact basin

C. BELL,[1] J. V. MORGAN,[1*] G. J. HAMPSON,[1] and B. TRUDGILL[2]

[1]Department of Earth Science and Engineering, Imperial College London SW7 2AZ, UK
[2]Department of Geology and Geological Engineering, Colorado School of Mines, Colorado 80401, USA
[*]Corresponding author. E-mail: j.v.morgan@imperial.ac.uk

(Received 15 July 2003; revision accepted 21 April 2004)

Abstract–Seismic data across the offshore half of the Chicxulub impact crater reveal a 145 km-diameter post-impact basin to be a thickening of Tertiary sediment, which thickens by ~0.7 sec from the basin margin to the basin center. The basin existed long after the impact and was gradually infilled to its current flat surface. A suite of seismic horizons within the impact basin have been picked on four reflection lines across the crater. They reveal that the western and northwestern parts of the impact basin were filled first. Subsequently, there was a dramatic change in the depositional environment, indicated by an unconformable surface that can be mapped across the entire basin. A prograding shelf sequence downlaps onto this unconformity in the eastern basin. The seismic stratigraphic relationships suggest a marine regression, with sedimentation becoming gradually more passive as sediments fill the eastern part of the impact basin. The central and northeastern parts of the basin are filled last.

The onshore hole Yaxcopoil-1 (Yax-1), which was drilled on the flanks of the southern basin, has been projected onto the offshore seismic data to the west of the crater center. Using dates obtained from this onshore well and regional data, approximate ages have been placed on the most significant horizons in the offshore seismic data. Our preliminary interpretation is that the western and northwestern basins were almost entirely filled by 40 Ma and that the marine regression observed in the eastern basin is early Miocene in age. Offshore seismic stratigraphic analyses and onshore data within Yax-1 suggest that the early Paleocene is highly attenuated across the impact basin. The Mesozoic section appears to be ~1 km thicker offshore than onshore. We calculate that, given this offshore thickening, the volume of Mesozoic rocks that have been excavated, melted, or vaporized during impact is around 15% larger than expected from calculations that assume the offshore thickness is equal to that onshore. This has significant consequences for any environmental calculations. The current offset between the K-T boundary outside and inside the crater is ~700 m. However, infilling of basins with sediments is usually accompanied by subsidence, and immediately following the impact, the difference would have been smaller. We calculate the original topographic offset on the K-T boundary to have been between 450 and 700 m, which is in agreement with depth-diameter scaling laws for a mixed target.

INTRODUCTION

The British Institutions Reflection Profiling Syndicate (BIRPS) acquired ~650 km of a marine seismic reflection profile across the crater (Chicx-A, A1, B, and C in Fig. 1) in 1996. Seismic data were recorded to 18 sec two-way travel-time (TWTT) on a 240-channel 6 km streamer using a 50 m shot spacing. The reflection data have been published in Morgan et al. (1997) and Morgan and Warner (1999). Figure 2 shows a section of the seismic data along Chicx-A and A1. Closely-spaced high frequency reflectors within the impact basin between 0 and 1 sec TWTT are labeled as Tertiary, and those outside the basin between 0.5 and 2.5 sec are labelled as Mesozoic. These interpretations are based on comparisons with onshore well data and were used by Camargo-Zanoguera and Suárez-Reynoso (1994) in their interpretation of seismic reflection data acquired by PeMex (Petróleos Mexicanos). These data reveal a basin with an ~80 km-diameter topographic ring that appears analogous to peak rings observed on other planetary bodies (Grieve and Therriault 2004). We use the peak ring to divide the impact basin into two regions: the central basin and annular trough (Fig. 2).

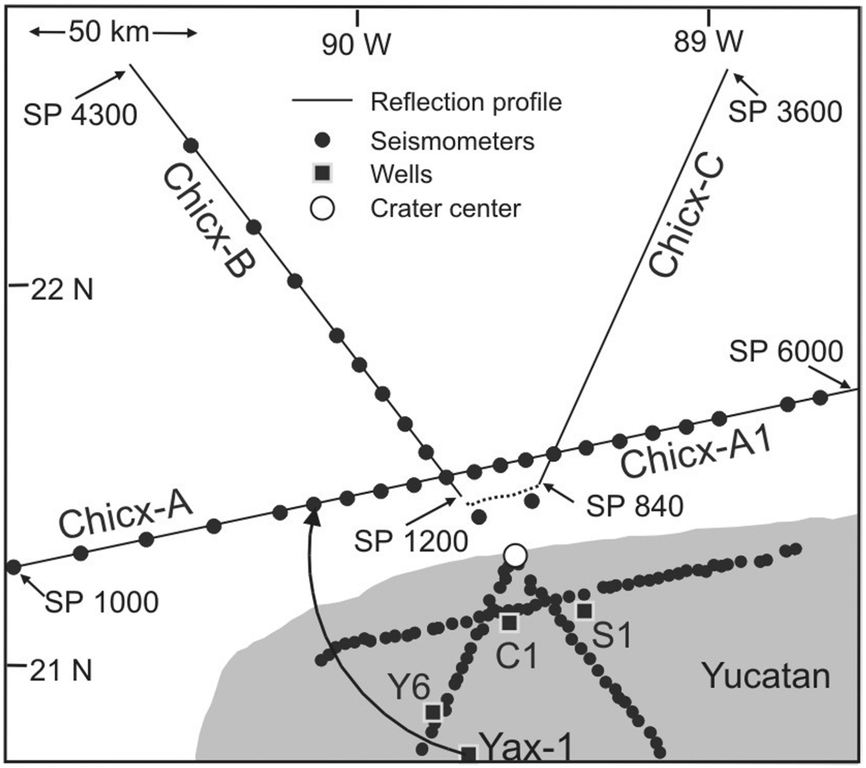

Fig. 1. A map showing the location of the BIRPS seismic reflection profiles and onshore drill holes within the impact basin: Yax-1, C1, S1, and Y6. The arrow leading from Yax-1 indicates the projection of this borehole on to seismic line Chicx-A. SP is a shotpoint number.

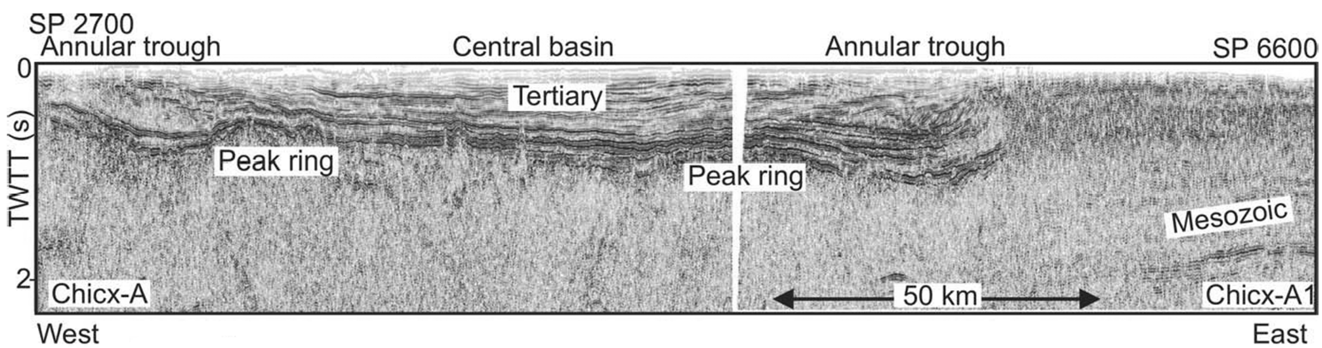

Fig. 2. Seismic reflection profile along part of Chicx-A and -A1; see the shotpoint map (Fig. 1) for location. The post-impact sediments are identified as high frequency reflections from 0 to ~1 sec TWTT. We refer to the area inside the peak ring as the central basin and the area outside the peak ring as the annular trough.

In the first half of this paper, we investigate post-impact sedimentation within the impact basin. Seismic horizons have been tracked across the crater on the four BIRPS lines. To define points of change in the depositional environment, as well as a detailed stratigraphy of sediment infill, many seismic horizons have been picked. However, in our interpretations, we bear in mind that we have 2D data and cannot represent 3D structure accurately. We then introduce onshore borehole Yax-1 and use stratigraphic data from this borehole and regional observations to assign preliminary ages to our main seismic horizons. In the discussion, we summarize some observations that have arisen from this work.

HORIZON PICKING AND INFILL INTERPRETATIONS

The program Seisworks was used for horizon picking. The horizons have been picked by starting at the point where the reflector has the strongest amplitude, and once picked, each horizon is then highlighted with a particular color. Picking a horizon may be done by "point picking," where the interpreter chooses the points on the line, or by "auto picking," where Seisworks uses either dip or amplitude to pick the horizon. Both of these methods were employed. Auto picking worked best where reflectors have high amplitudes

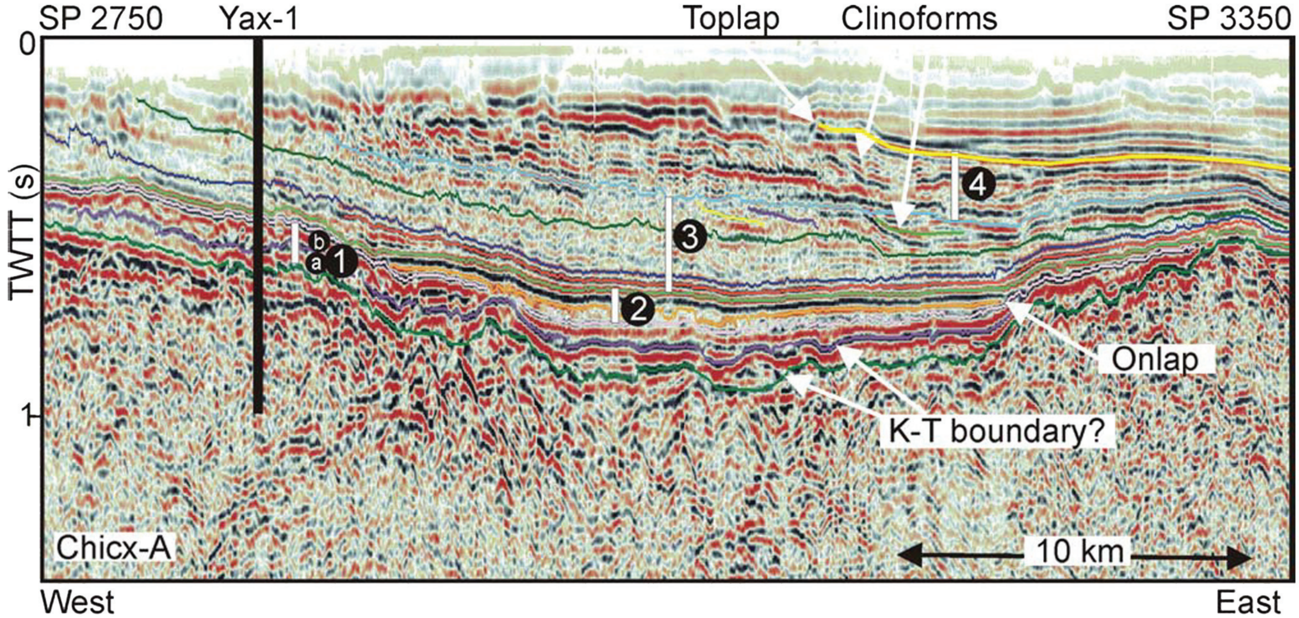

Fig. 3. Closeup of picked horizons on the seismic reflection profile across the western annular trough on Chicx-A. See the shotpoint map (Fig. 1) for the location. The white bars and numbers indicate the location of the four picked stratal units; unit 1 is split into packages a and b. Yax-1 shows the projected location of the onshore borehole (see Fig. 1 for projection).

and are continuous. Point picking was necessary where reflectors were discontinuous or where reflection amplitudes showed rapid lateral variations.

Seismic stratigraphic methods, which are based on variations in seismic facies (e.g., reflector amplitude, continuity, configuration) and reflector geometries and terminations (see papers in Vail et al. [1977]), were used to divide the Tertiary stratigraphy into the stratal packages described below. The K-T boundary was chosen with the assumption that the base of the high frequency reflectors represented the earliest Tertiary sediments; the picked boundary is in broad agreement with onshore borehole data (Ward et al. 1995; Sharpton et al. 1996). By K-T boundary, we mean the point after which Paleocene sediments are first deposited. We recognize that there is some ambiguity in the precise choice of this horizon, particularly as impact breccia deposits can be layered and may have a similar seismic character to Paleocene sediments. To better illustrate the horizon picking, we start with closeups of the data.

Western Annular Trough

The western annular trough is shown in Fig. 3. The range of possible horizons for the K-T boundary are picked in the lower part of unit 1. Our preferred K-T boundary reflector is highlighted in green in Fig. 3 but may well correspond to the next picked reflector highlighted in dark purple or somewhere between the two (Fig. 3). On the basis of changes in seismic facies and reflector configurations, the western margin has been split into four stratal units. Unit 1 contains the first few reflectors that are broadly concordant with the picked K-T boundary (between green and pink horizons). Unit 1 can be subdivided into lower and upper parts (a and b, respectively, in Fig. 3) that are separated by the dark purple reflector (highlighted as the upper potential K-T boundary reflector in Fig. 3); reflectors in the upper part of unit 1 onlap the purple reflector around a local high in the western part of the trough. Unit 2 consists of strong continuous sub-horizontal reflectors, several of which onlap the top reflector of unit 1 toward both the western and eastern margins of the trough (see Fig. 3). This reflector configuration indicates that the deepest part of the annular trough contains the thickest section of earliest basin-fill strata.

Unit 3 comprises a series of discontinuous, low amplitude reflectors (between light green and light blue horizons). The boundary between units 2 and 3 follows the shape of the K-T boundary. The upper part of this third unit contains a package of parallel, eastward-dipping clinoforms dipping at 3–4° that downlap onto a continuous horizon within the unit (Fig. 3). Clinoform reflectors show toplap, and the overall clinoform package extends ~23 km from west to east. Unit 3 wedges out toward the east, suggesting that it has been deposited from the west. The clinoforms within this unit also indicate overall progradation of a slope toward the east. Clinoform height can be used to indicate paleo-water depth (White et al. 1992), with the assumption that the tops of the clinoforms were approximately at sea-level. Here, the clinoforms suggest a paleo-water depth of ~100 m.

Unit 4 consists mainly of strong continuous reflectors that are interspersed with poorly defined packages of

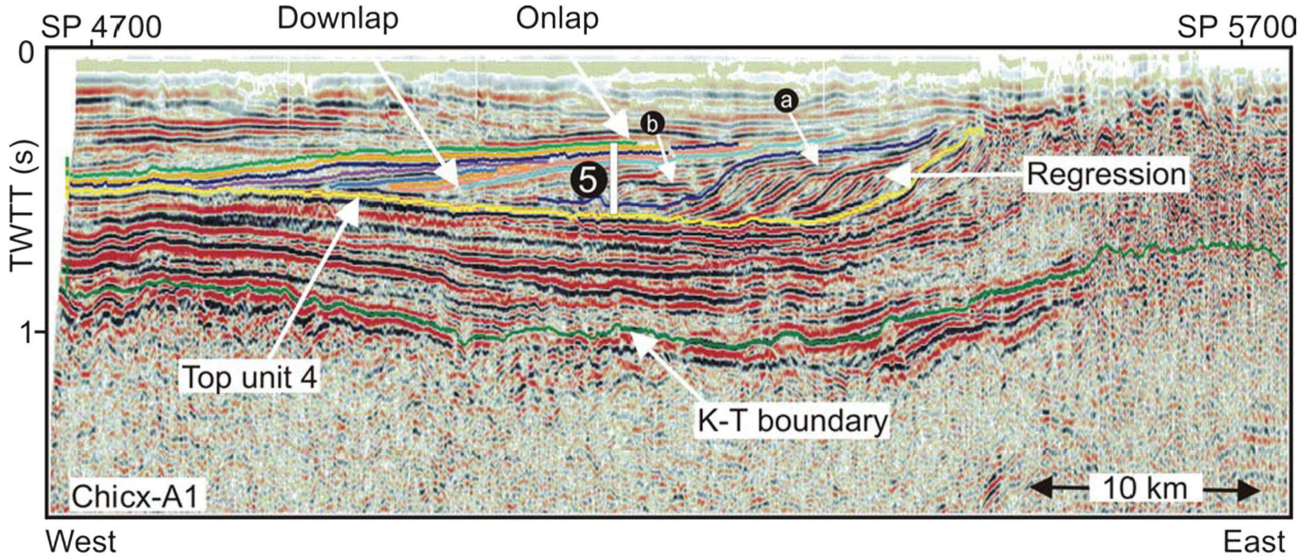

Fig. 4. Closeup of picked horizons on the seismic reflection profile across the eastern annular trough on Chicx-A1. See the shotpoint map (Fig. 1) for the location. The white bar indicates the location of stratal unit 5; unit 5 is split into packages a and b.

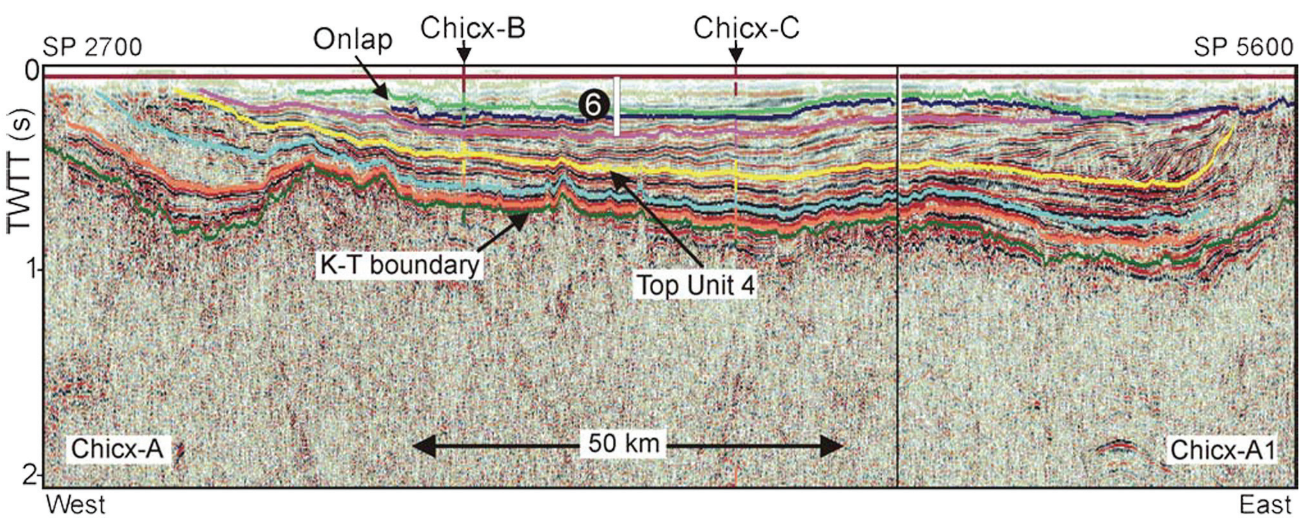

Fig. 5. Picked horizons across the impact basin on the seismic reflection profiles Chicx-A and -A1. See the shotpoint map (Fig. 1) for the location. The white bar indicates the location of picked stratal unit 6. Chicx-B and Chicx-C indicate the positions where these lines cross Chicx-A and -A1.

eastward-dipping clinoforms. Strong continuous reflectors in the upper part of unit 4 display apparent angular truncation or toplap at the uppermost reflection surface of the unit (see Fig. 3). The top of unit 4 (yellow reflector) provides a major marker boundary for a change in depositional environment across the basin that is most clearly observed in the eastern annular trough on Chicx-A1 (see Fig. 4).

Eastern Annular Trough

The eastern margin shows a very different infill history from that of the western trough (Fig. 4). Reflectors from units 1, 3, and 4 may be traced from Chicx-A to -A1, and they are all concordant with the reflector interpreted as the K-T boundary (Fig. 5). The boundary between units 4 and 5 (reflector colored yellow) reveals a major change in deposition. In the eastern margin, reflectors in unit 5 downlap on to the top reflector of unit 4.

Unit 5 consists of a series of reflectors with complex geometries that are well-resolved in the data. The first reflectors deposited on the edge of the eastern basin possess the geometry of relatively steep (5–8°), westward-dipping sigmoid-oblique clinoforms (between yellow and dark blue horizons, labeled [a] in Fig. 4). Within this clinoform package, the older clinoform reflectors exhibit successive offlap from one another. The overall geometry is typical of a prograding slope, while the offlap relationship indicates regression during falling relative sea-level. This package is overlain by a second clinoform package, in which reflectors exhibit much shallower dips (1–2°) and parallel geometries (between two dark blue horizons, labeled [b] in Fig. 4). The lower part of this second clinoform package contains discontinuous, low-amplitude reflectors with poorly resolved chaotic and mounded geometries that suggest a mass flow deposit resulting from collapse of the underlying, steeper clinoform unit. The decrease in westward dip between the first and second clinoform packages is consistent with either a paleogeographic re-orientation of the clinoform/slope system or evolution to a gentler slope after mass wasting. Deposition of these two clinoform packages is likely to correspond to relatively fast sedimentation. Reflectors immediately above the two packages show draping and onlap of the clinoform surfaces, indicative of a more passive stage of sedimentation, or a further paleogeographic re-orientation of the clinoform/slope system (see mustard yellow and bright green reflectors in Fig. 4). As unit 5 thins toward the west and contains westward-dipping clinoforms, it is likely that this unit was deposited from the east.

There are no lithological data to constrain the nature of the clinoform/slope systems in the western margin of units 3 and 4 (Fig. 3) or the eastern margin of unit 5 (Fig. 4). However, their scale, 2D geometry, and seismic facies character are suggestive of either a siliciclastic delta system, which typically exhibits clinoform/delta front dips of 1–5°, or a gentle, non-reefal carbonate slope such as that developed at the leeward margin of the Bahamas platform (2–6° clinoform/slope dip; Eberli and Ginsburg 1987). Either interpretation implies infilling of significant bathymetry within the eastern part of the crater basin during deposition of unit 5, where the height of the clinoforms implies an approximate paleo-water depth of 350 m. A carbonate slope interpretation appears more consistent with sparse onshore data that suggest an absence of Tertiary siliciclastic sediment (Galloway et al. 1991) and implies that crater bathymetry was infilled by the growth and coalescence of separate carbonate platforms in a manner directly analogous to the formation of the Great Bahama Bank (Eberli and Ginsburg 1987). Alternatively, a deltaic interpretation for one or more clinoform packages implies widespread emergence and bypass of siliciclastic sediment across the Yucatán platform, consistent with development of a sequence boundary during a relative sea-level lowstand.

Onshore data indicate that a widespread unconformity was developed across the shallower part of the Yucatán platform during the late Oligocene to early Miocene, probably caused by a pronounced relative sea-level fall (Galloway et al. 1991). We speculate that this base-Miocene unconformity may correlate to the offlapping clinoform/slope geometries observed in the lower part of unit 5, which record a net relative sea-level fall of 50–100 m during clinoform/slope regression. This would give an approximate age of 23 Ma for the lower part of unit 5. Provisional biostratigraphic work from the Campeche Shelf, west of the Yucatán Peninsula, indicates unconformities across the Paleocene-Eocene boundary, the Eocene-Oligocene boundary, and most markedly, across the middle- to upper-Miocene boundary (Medina 2001). Correlating this last unconformity to the offlapping clinoform/slope package implies an age range of 10–15 Ma for the lower part of unit 5.

Central Basin

Unit 6 consists of strong, continuous, parallel reflectors, and it infills the remaining space within the crater. Reflectors within the unit are traceable through Chicx-A1 into the west of Chicx-A, and they onlap the top of unit 5 at the western and eastern basin margins (Fig. 5). Overall, unit 6 records passive, sub-horizontal sediment infill marking the final stage of deposition along Chicx-A and -A1.

Chicx-B and -C

Figure 6 shows a selection of horizons picked along Chicx-B and Chicx-C. Chicx-B shows a similar pattern of basin infill to Chicx-A, indicating that the northwestern and western annular troughs were filled before the eastern trough. Unlike on other lines, on Chicx-C, the Tertiary thickens outside the impact basin (see the strata above the picked K-T boundary reflector, bottom green horizon). Note also that the depth to the top of unit 4 (yellow reflector) increases to the northeast of the impact basin.

YAXCOPOIL-1

As there are no offshore drill holes close by, Yax-1 is currently the best source for stratigraphic data within the impact basin. Yax-1 was cored between 400 and 1500 m. Cretaceous rocks were drilled between ~900 and 1500 m, impactites between ~800 and 900 m, and Tertiary rocks above ~794 m (Dressler et al. 2003; Arz et al. 2004; Keller et al. 2004). The onshore borehole Yax-1 has been projected along a line of constant radius onto the seismic data in the western basin (see Figs. 1 and 3). We use this projection because the offshore/onshore potential field data are more comparable in this direction than to the east of the crater (Sharpton et al. 1996; Hildebrand et al. 1998). However, we recognize that this is a long way to project stratigraphic data, especially given the observed variation in the offshore seismic stratigraphy in different directions (Figs. 3–6).

Figure 7 summarizes the results from the horizon picking. In Fig. 7a, the six interpreted stratal units are shown, as well as the projected location of Yax-1. Two-way travel-time has been converted to depth using seismic refraction velocities of Christeson et al. (1999) and Morgan et al. (2002). We note that the depth to the K-T boundary in Yax-1 is the same as that calculated for Chicx-A at the same radial distance (~800 m). Thus, as far as we can tell, the gradual thickening of the

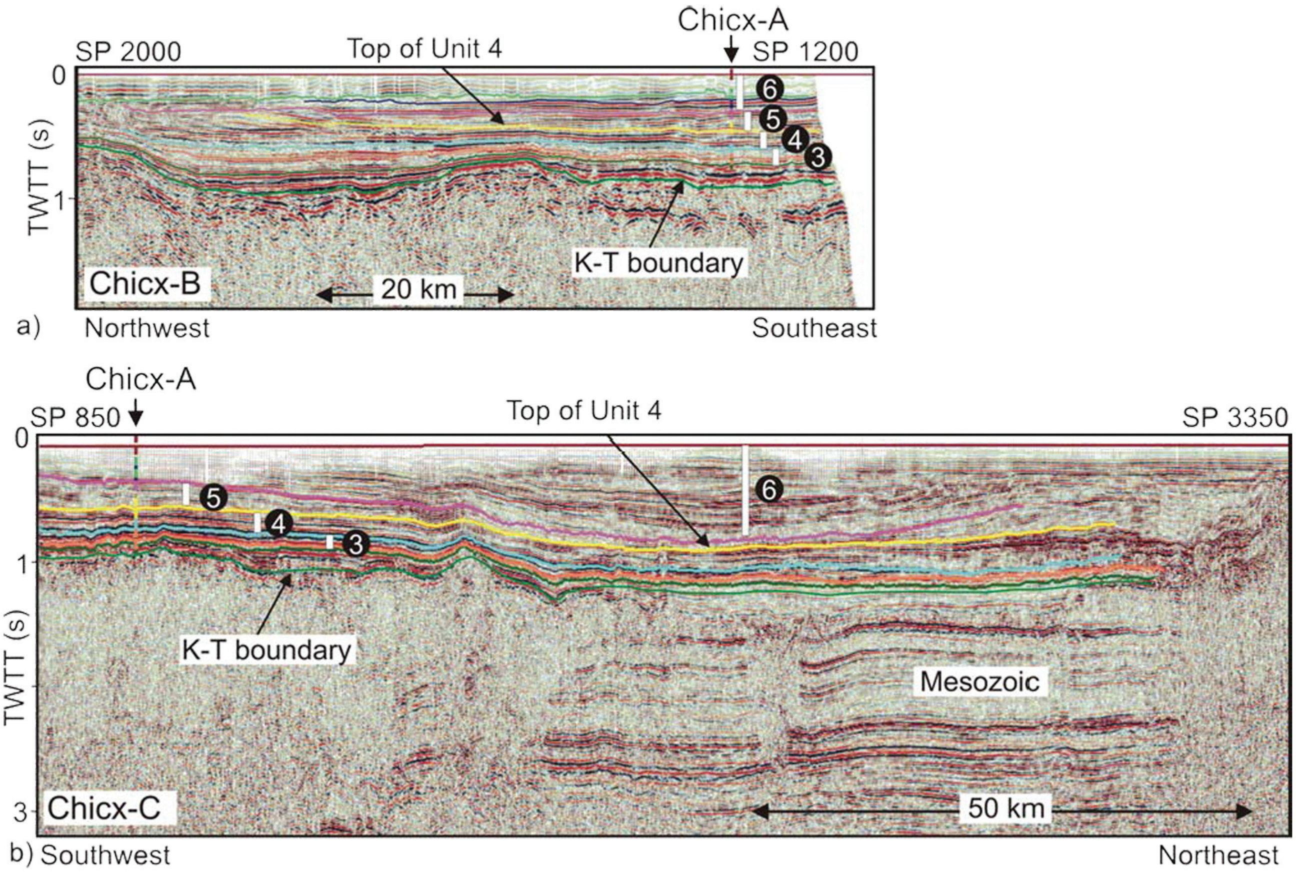

Fig. 6. Picked horizons across the impact basin on seismic reflection profiles Chicx-B and -C. See the shotpoint map (Fig. 1) for the location. The white bars and numbers indicate the location of picked stratal units. Chicx-A indicates the positions where this line crosses Chicx-B and -C.

Tertiary section observed offshore (Fig. 2) is in agreement with all the onshore well data. In Fig. 7b, dates have been assigned to some of the boundaries using stratigraphic data from Yax-1 and regional data. To date, stratigraphic ages in the Tertiary rocks have been provided for the top of the Yax-1 core by Smit et al. (2004) and at the base of the Tertiary by Stinnesbeck et al. (2003), Smit et al. (2004), Arz et al. (2004), and Keller et al. (2004). As discussed above, we interpret the K-T boundary to be one of a sequence of reflectors that we labeled as unit 1 and, thus, assign an age of 65 Ma to this unit. Lower Paleocene fossils are observed between ~780 and 794 m in Yax-1, and from our projection of Yax-1 onto the seismic data (Fig. 7a), this unit is intersected at ~800 m. Yax-1 samples between 400–450 m have been dated as lower to middle Eocene (40.2–43.5 Ma) by Smit et al. (2004). The base of unit 4 occurs at a depth of ~360 m (Fig. 7a), and using our projection of Yax-1, we have assigned a provisional age of ~40 Ma (rounded to the nearest 5 Ma) to this boundary. Note that this assumes that the crater has a similar infill history in the southern and westerly parts of the basin. Using regional data, we interpret the oldest sediments in unit 5 to be ~23 Ma, as they represent a likely correlative to a widespread unconformity of this age developed onshore (Galloway et al. 1991). An alternative correlation of these strata to an unconformity on the Campeche shelf (Medina 2001) provides an age of 10–15 Ma for their deposition. Given the distance that we are projecting for the Yax-1 stratigraphic data, as well as the sparse nature of the regional data, we emphasize that our dating is preliminary at best.

DISCUSSION

Our seismic stratigraphic analyses indicate that the impact basin was gradually infilled to its current flat surface. The western and northwestern parts of the impact basin were filled first. Subsequently, there was a dramatic change in depositional environment, indicated by an unconformable surface that can be mapped across the entire basin. A prograding shelf sequence downlaps on to this unconformity in the eastern basin. The seismic stratigraphic relationships suggest a marine regression, with sedimentation becoming gradually more passive as sediments fill the eastern part of the impact basin. The central and northeastern parts of the basin were filled last.

Thickness of the Early Paleocene Section

Offshore, the thickest sequence of early crater fill

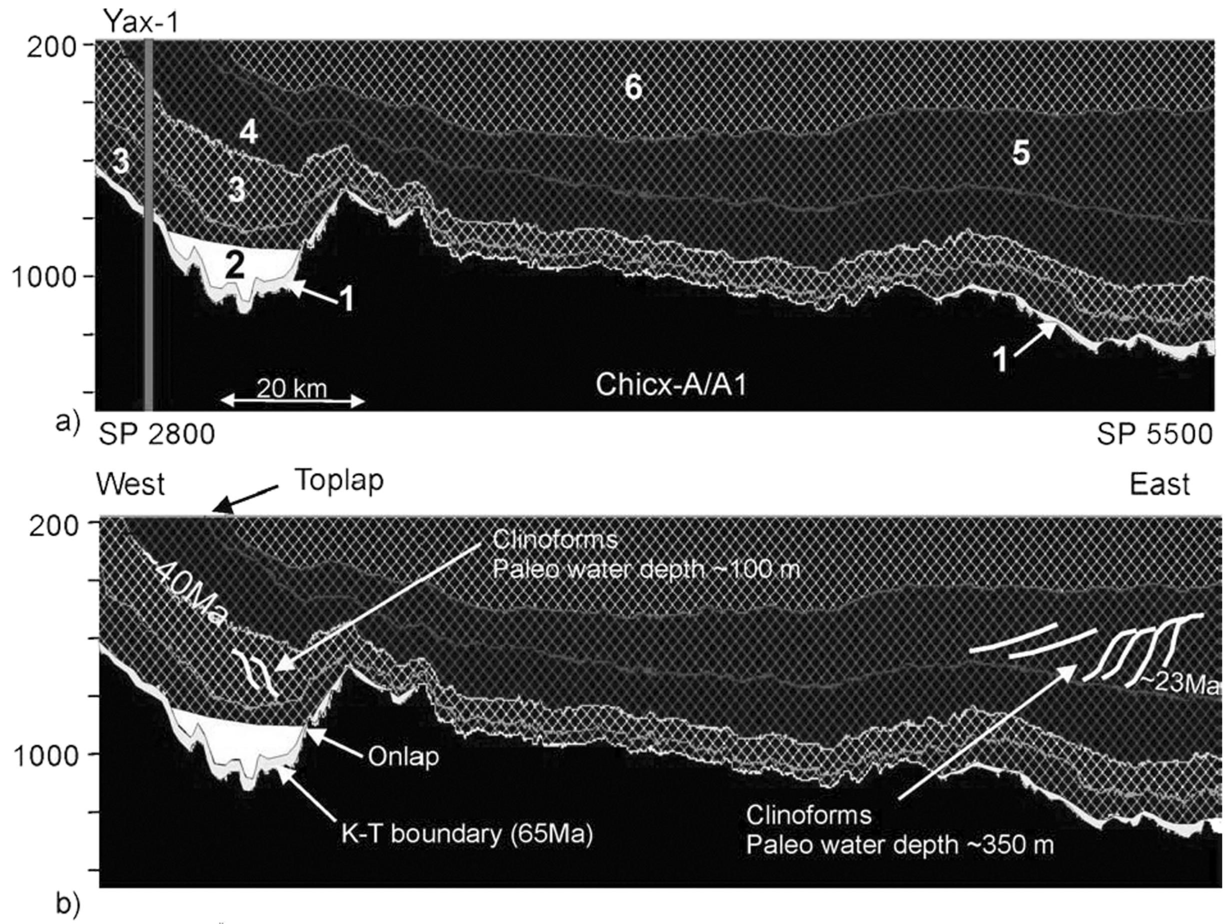

Fig. 7. a) Summary of the six picked stratal units along Chicx-A and -A1 displayed in depth. See the shotpoint map (see Fig. 1) for the location; b) as (a) but with approximate ages on some boundaries. See text for details.

deposits lie in the deepest part of the western basin (unit 2 in Fig. 7a), and these deposits onlap the interpreted location of the K-T boundary (unit 1). This reflector configuration indicates that unit 2 is likely to be early Paleocene in age and that, outside of the deepest part of the western trough, we might expect rocks of this age to be attenuated or missing. However, we note that the vertical resolution of seismic data at this depth is ~25 m, and we cannot identify packages of beds that are significantly thinner than this. Biostratigraphic data in Yax-1 reveal a highly condensed Danian section (Stinnesbeck et al. 2003; Arz et al. 2004; Keller et al. 2004), which is supported by the switch from magnetochron 29r to 29N a few cm after the first Tertiary fossils appear (Rebolledo-Vieyra et al. 2004). In conclusion, offshore seismic stratigraphic analyses and onshore data within Yax-1 suggest that the early Paleocene might be highly condensed across the impact basin.

Thickness of the Mesozoic Section

One notable observation from the marine seismic reflection data is that the Cretaceous sediments are almost certainly thicker offshore than onshore. Figure 8 shows the thickness of the Mesozoic section in the onshore wells, although the entire section has only been penetrated in well Y1. Offshore, we show the calculated thickness of the Mesozoic rocks outside of any major disruption of the target rocks. The TWTT through the section interpreted as Mesozoic on lines Chicx-A, -A1, -B, -C, PeMex-1, and -2 varies between 1.3 and 1.4 sec. We have converted reflection times to depths using velocities from cores and sonic logs in Yax-1. Velocity varies within the various Cretaceous lithologies: the calcarenites in Yax-1 have velocities between 4.5 and 5.0 kms^{-1}, while the dolomites have velocities of around 6.2 kms^{-1} (Vermeesch and Morgan 2004). As Yax-1 penetrates target rocks that are likely to have been disturbed by the impact, we might expect the velocities in these rocks to be slightly lower than those further out from the center. We have used an average velocity for the Mesozoic section of 5.4 kms^{-1}, but the average velocity could realistically vary between 5.2 and 5.6 kms^{-1}, depending on precise lithology. This range of values is consistent with velocity models obtained from seismic refraction data (Christeson et al. 1999). Using these velocities, the offshore thickness of the Mesozoic

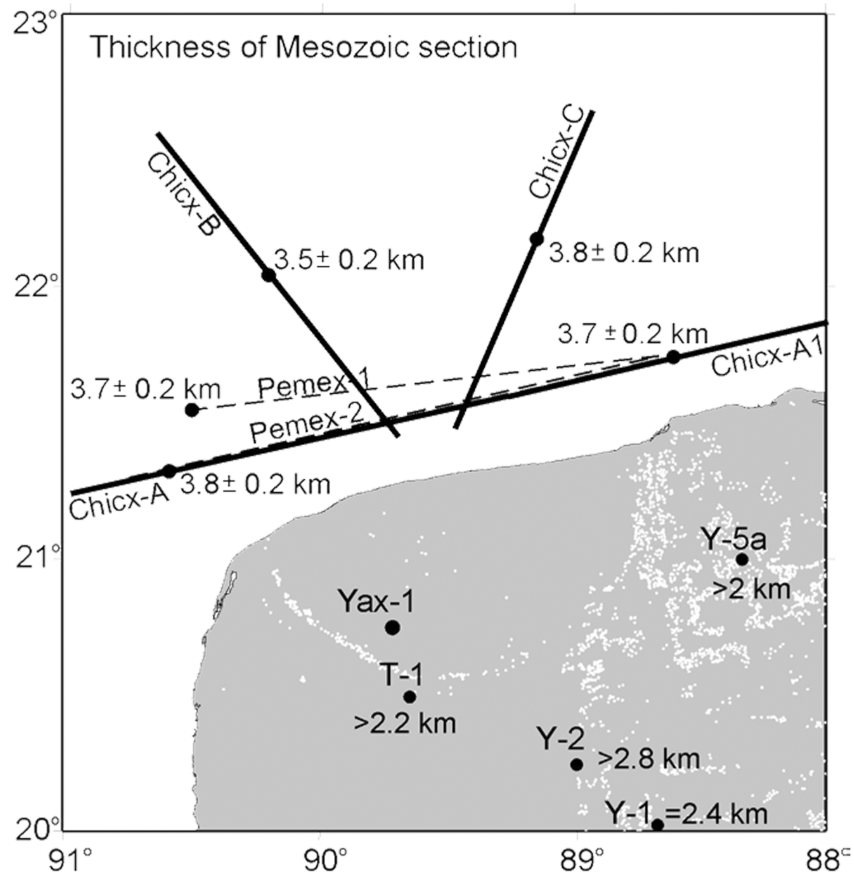

Fig. 8. Map showing the estimated thickness of the Mesozoic section from seismic reflection profiles and the measured Mesozoic thickness in onshore wells.

along the reflection profiles is 3.5 to 3.8 ± 0.2 km (Fig. 8). These calculations suggest that the Cretaceous sediments are thicker offshore than onshore.

The observed increase in thickness of the Mesozoic section offshore has implications for the environmental effect of this impact. The Chicxulub impact may have been particularly lethal because the lithologic composition of the target sediments caused large volumes of carbon and sulfur to be released (e.g., O'Keefe and Ahrens 1989; Sigurdsson et al. 1992). As the depth of excavation should be greater than 10 km for a crater of this size (e.g., Melosh 1989), the entire Mesozoic section would have been involved in the impact. Hence, the thicker the Mesozoic sedimentary layer, the greater the volume of potential pollutants released. Current estimates for sedimentary thickness based on onshore data are between 2.5 and 3.0 km (Camargo-Zanoguera and Suárez-Reynosa 1994; Ward et al. 1994; Sharpton et al. 1996), but offshore, the thickness is about 1 km (30%) thicker (Fig. 8). From this, we can say that the total volume of sediments that have been shocked, melted, and excavated by this impact is likely to have been 15% larger than expected from calculations that assume the offshore thickness was the same as that measured in onshore data.

Scaling Laws

Scaling laws for terrestrial craters are hard to determine because of post-impact erosion (particularly of the crater rim), infilling of the impact basin, and other effects. Using observations from craters on Earth, Grieve and Pesonen (1992) published two scaling laws for complex terrestrial craters:

$$H = 0.12D^{0.3} \qquad \text{(sedimentary target)}$$
$$H = 0.15D^{0.43} \qquad \text{(crystalline target)}$$

where D is the diameter of the crater, and H is the apparent crater depth (Fig. 9a). Although the first 3 km of the Yucatán target is sedimentary, this is a large impact, and the crystalline rocks are also likely to control the final crater form. At Chicxulub, the crater rim has been eroded (Fig. 9b), and we cannot determine H or the rim height (h_r) directly, but we can measure H-h_r. The crater diameter is estimated to be 190 ± 10 km (Morgan et al. 1997; Hildebrand et al. 1998; Dressler et al. 2003). Using this diameter in the equations above, the expected apparent crater depth (H) would be 600 m for a sedimentary target and 1400 m for a crystalline one. No scaling laws for rim height (h_r) have been put forward for terrestrial craters, but for complex craters on the Moon, the

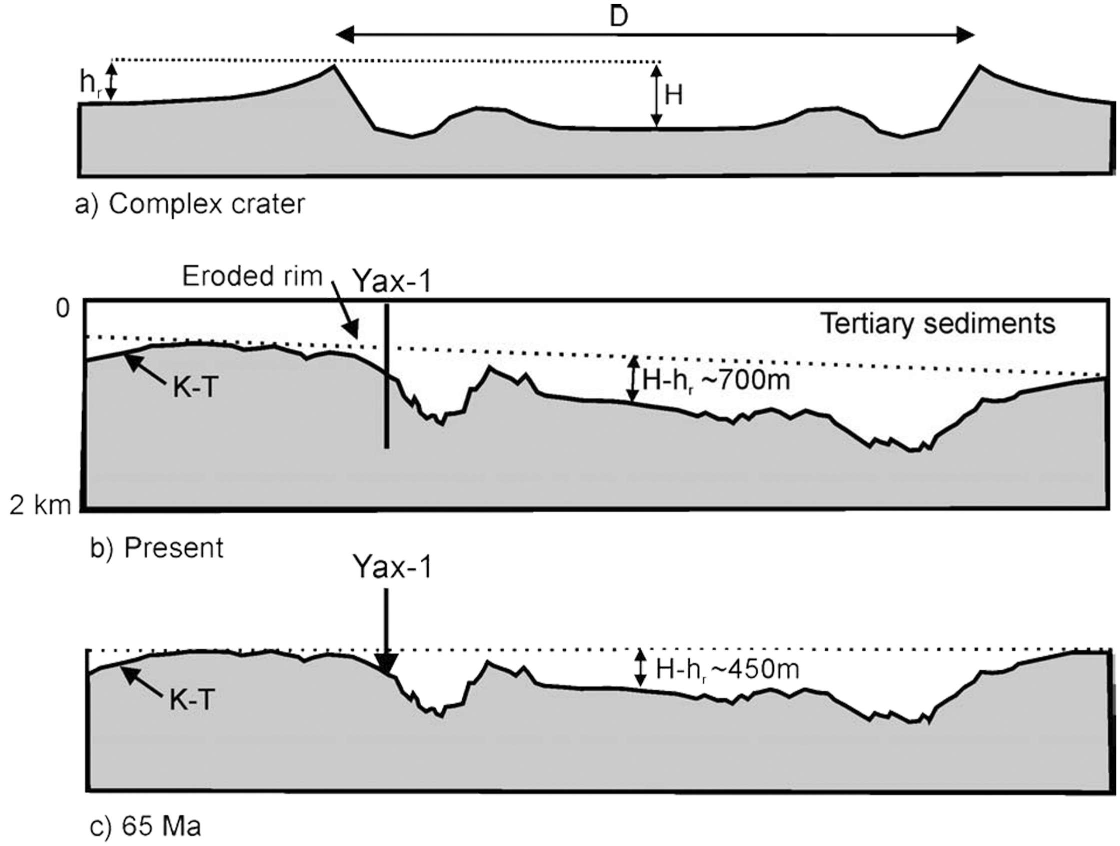

Fig. 9. a) A profile across a complex crater that illustrates the measurements used in scaling laws: D is crater diameter, H is crater depth, and h_r is the height of the crater rim; b) current depth to the K-T boundary from seismic reflection profiles Chicx-A and -A1. Yax-1 shows the projected location of the onshore borehole (see Fig. 1 for projection). The dotted line represents the approximate location of the K-T boundary outside the impact basin; H-h_r represents the current offset in the K-T boundary. Note that the original crater rim has been eroded; c) topography across the crater 65 Ma. The effects of post-impact subsidence due to sediment loading have been removed, as has the regional tilt from west to east. The dotted line represents the approximate location of the K-T boundary outside the impact basin; H-h_r represents the minimum original offset in the K-T boundary.

ratio of H/h_r is ~2.6 (Pike 1977). The ratio is likely to be similar on Earth, giving h_r values of ~350 and ~550 m and H-h_r values of 250 and 850 m for sedimentary and crystalline targets, respectively.

The current K-T boundary has an average topography of about 700 m (Ebbing et al. 2001) between the outside and inside of the impact basin (Fig. 9b). As sediments infill tectonic basins, they subside. This is equally likely to occur within an impact basin. The extra load of the infilling sediments will push the crater floor down and increase the topographic offset between the K-T boundary inside and outside the basin. For small basins, the crust can have enough strength to resist subsidence, but for an impact basin the size of Chicxulub, gravitational forces are likely to drive some subsidence. If we make the assumption that the crust has no strength, we can calculate the maximum expected subsidence that would occur if the basin remained in isostatic equilibrium. The average density of Tertiary platform carbonates outside the basin is ~2.4 ± 0.1 g/cm^{-3}, while the average density of the deep water Tertiary marls and carbonates is ~2.1 ± 0.1 g/cm^{-3} (Vermeesch and Morgan 2004). We have calculated the effect of back-stripping the post-impact sediments from outside and inside the impact (i.e., removing 500 m and 1200 m load from these two areas, respectively) on crater topography. Our calculations use the key assumptions that the basin was filled with water and was in isostatic equilibrium immediately after the impact. With these values and assumptions, the original topographic offset on the K-T boundary would have been around 450 m (Fig. 9c).

We propose that, immediately after impact at Chicxulub, H-h_r would have been between 450 and 700 m, and the precise value would depend upon the elastic thickness of the crust and the time constant for crustal relaxation. This range is in agreement with scaling laws and lies between the values calculated from the scaling laws above: 250 m for a sedimentary target and 850 m for a crystalline one.

Acknowledgments–This work forms part of the MSci dissertation of C. Bell, supported by the Department of Earth Science and Engineering at the Imperial College London. We thank the International Continental Drilling Program for funding the drilling of Yaxcopoil-1, and Jaime Urrutia-

Fucugauchi and Ana Maria Soler-Arechalde for overseeing the core sampling at Universidad Nacional Autónoma de México. The acquisition of the 1996 seismic data was funded by NERC and NSF.

Editorial Handling— Dr. Jaime Urrutia-Fucugauchi

REFERENCES

Arz J. A., Alegret L., and Arenillas I. 2004. Foraminiferal biostratigraphy and paleoenvironmental reconstruction at Yaxcopoil-1 drill hole, Chicxulub crater, Yucatán Peninsula. *Meteoritics & Planetary Science.* This issue.

Camargo-Zanoguera A. and Suárez-reynoso G. 1994. Evidencia sísmica del cráter impacto de Chicxulub. *Boletín de la Asociación Mexicana de Geofísicos de Exploración* 34:1–28.

Christeson G. L., Buffler R. T., and Nakamura Y. 1999. Upper crustal structure of the Chicxulub impact crater from wide-angle ocean bottom seismograph data. In *Large meteorite impacts and planetary evolution II,* edited by Dressler B. O. and Sharpton V. L. Special Paper 339. Boulder: Geological Society of America. pp. 291–305.

Dressler B. O., Sharpton V. L., Morgan J. V., Buffler R., Moran D., Smit J., Stöffler D., and Urrutia J. 2003. Investigating a 65-Ma-old smoking gun: Deep drilling of the Chicxulub impact structure. *Eos Transactions* 84:125, 130.

Eberli G. P. and Ginsburg R. N. 1987. Segmentation and coalescence of Cenozoic carbonate platforms, northwestern Great Bahama Bank. *Geology* 15:75–79.

Ebbing J., Janle P., Koulouris J., and Milkereit B. 2001. 3D gravity modeling of the Chicxulub impact structure. *Planetary and Space Science* 49:599–609.

Galloway W. E., Bebout D. G., Fisher W. L., Dunlap J. B., Jr., Cabrera-Castro R., Lugo-Rivera J. E., and Scott-Thomas M. 1991. Cenozoic. In *The Gulf of Mexico basin,* edited by Salvador-Amos. Boulder: Geological Society of America. pp. 245–324.

Grieve R. A. F. and Pesonen L. J. 1992. The terrestrial impact cratering record. *Tectonophysics* 216:1–30

Grieve R. A. F. and Therriault A. 2004. Observations at impact structures: What constraints have they provided on cratering processes. *Meteoritics & Planetary Science* 39:199–216.

Hildebrand A. R., Pilkington M., Ortiz-Aleman C., Chavez R. E., Urrutia-Fucugauchi J., Connors M., Graniel-Castro E., and Camargo-Zanoguera A. 1998. Mapping Chicxulub crater structure with gravity and seismic reflection data. In *Meteorites: Flux with time and impact effects,* edited by Grady M. M., Hutchinson R., McCall G. J. H., and Rothery D. A. Special Publication 140. London: Geological Society of London. pp. 177–193.

Keller G., Adatte T., Stinnesbeck W., Rebolledo-Vieyra M., and Urrutia-Fucugauchi J. 2004. Chicxulub impact predates the K-T boundary mass extinction. *Proceedings of the National Academy of Sciences* 101:3753–3758.

Medina G. S. 2001. Tertiary zonation based on Planktonic foraminifera from the marine region of Campeche, Mexico. In *The Western Gulf of Mexico basin: Tectonics, sedimentary, and petroleum systems,* edited by Bartolini C., Buffler R. T., and Cantj-Chapa A. Tulsa: American Association of Petroleum Geologists. pp. 397–420.

Melosh H. J. and Ivanov B. 1999. Impact crater collapse. *Annual Review of Earth and Planetary Sciences* 27:385–415.

Morgan J., Warner M., and Chicxulub Working Group. 1997. Size and morphology of the Chicxulub impact crater. *Nature* 390: 472–476.

Morgan J. and Warner M. 1999. The third dimension of a multi-ring impact basin. *Geology* 27:407–410.

Morgan J. V., Christeson G., and Zelt C. 2002. Testing the resolution of a 3D velocity tomogram across the Chicxulub crater. *Tectonophysics* 355:215–226.

O'Keefe J. and Ahrens T. 1989. Impact production of CO_2 by the extinction bollide and the resultant heating of the Earth. *Nature* 338:247–249.

Pike R. J. 1977. Size-dependence on the shape of fresh impact craters on the moon. In *Impact and explosion cratering,* edited by Roddy D. J., Pepin R. O., and Merril R. B. New York: Pergamon Press. pp. 489–509.

Rebolledo-Vieyra M. and Urrutia-Fucugauchi J. 2004. Magnetostratigraphy of the impact breccias and post-impact carbonates from borehole Yaxcopoil-1, Chicxulub impact crater, Yucatán, Mexico. *Meteoritics & Planetary Science* 39:821–829.

Sigurdsson H., Dhondt S., and Carey S. 1992. The impact of the Cretaceous/Tertiary bolide on evaporite terrane and generation of major sulfuric acid aerosol. *Earth and Planetary Science Letters* 109:543–559.

Sharpton V. L., Marin L. E., Carney J. L., Lee S., Ryder G., Schuraytz B. C., Sikora P., and Spudis P. D. 1996. Model of the Chicxulub impact basin. In *The Cretaceous-Tertiary event and other catastrophes in Earth history,* edited by Ryder G., Fastovsky D., and Gartner S. Special Paper 307. Boulder: Geological Society of America. pp. 55–74.

Smit J., van der Gaast S., and Lustenhouwer W. 2004. Is the transition impact to post-impact rock complete? Some remarks based on XRF scanning, electron microbe, and thin section analyses of the Yaxcopoil-1 core in the Chicxulub crater. *Meteoritics & Planetary Science*. This issue.

Stinnesbeck W., Keller G., Adatte T., Harting M., and Stüben D. 2003. Yaxcopoil-1 and the Chicxulub impact (abstract #4037). In *Large meteorite impacts.* LPI Contribution No 1167. Houston: Lunar and Planetary Institute.

Vail P. R., Mitchum R. M., Jr., and Thompson S., III. 1977. Seismic stratigraphy and global changes in sea level. Part three: Relative changes of sea level from coastal onlap. In *Seismic stratigraphy: Applications to hydrocarbon exploration,* edited by Payton C. E. Tulsa: American Association of Petroleum Geologists. pp. 63–83.

Vermeesch P. M. and Morgan J. V. 2004. Chicxulub central crater structure: Initial results from physical property measurements and combined velocity and gravity modeling. *Meteoritics & Planetary Science.* This issue.

Ward W. C., Keller G., Stinnesbeck W., and Adatte T. 1995. Yucatán subsurface stratigraphy: Implications and constraints for the Chicxulub and constraints for the Chicxulub impact. *Geology* 23: 873–876.

White J. D. L. 1992. Pliocene subaqueous fans and Gilbert-type deltas in maar crater lakes, Hopi Buttes, Navajo Nation (Arizona), USA. *Sedimentology* 39:931–946.